Swirl Characteristics of Vortex Valve Variable-Thrust Solid Rocket Motor

X. G. Wei[†], J. Li and G. Q. He

Science and Technology on Combustion, Internal Flow and Thermal-structure Laboratory，Northwestern Polytechnical University, Xi'an, 710072, P.R. China

†*Corresponding Author Email: realysnow@nwpu.edu.cn*

ABSTRACT

In accordance with the flow characteristics of vortex valve variable-thrust solid rocket motors, a cold flow experimental system based on Particle Image Velocimetry was established. A flow velocity vector diagram of vortex chamber was generated, and the vortex structure was analyzed. The results provided an experimental foundation for numerical simulation. The flow characteristics in vortex chamber and in the throat and divergent sections of the nozzle were modeled and simulated. The flow in the vortex chamber conformed to the complex Rankine vortex, and the flow field was divided into three different zones. The vortex core was the primary influence factor for thrust modulation. The resultant velocity reached Mach number 1 before gas arrived at nozzle throat, and the axial velocity still reached Mach number 1 at nozzle throat. Hence, the axial velocity can be used to judge the occurrence of choking at the nozzle throat. The intensity of swirl flow in divergent section of the nozzle was evidently lower than that in vortex chamber and throat. As a result, a low-pressure zone emerged around the central axis, thereby causing thrust losses.

NOMENCLATURE

A_p	area of propellant combustion surface	r	burning rate
a	burning rate constant	SRM	Solid Rocket Motor
CFD	Computation Fluid Dynamics	SST	Shear-Stress Transport
k	the turbulence kinetic energy	T_f	the combustion temperature of the propellant
Ma	mach number of the throat		
Ma_X	the axial Mach number of the throat	UDF	User-Defined Functions
NASA	National Aeronautics and Space Administration		
n	the burning rate pressure exponent	$\dot{m}$	mass flow rate
PIV	Particle Image Velocimetry	ω	specific dissipation rate
p_c	the pressure of combustion chamber	ρ_p	density of solid propellant

1. INTRODUCTION

An effective method to achieve thrust modulation in solid propellant rocket motors is the adoption of vortex valve. A vortex valve is a fluid control component without moving parts. It achieves thrust modulation by spraying fluid into the motor along the tangential direction of flow field to force the combustion gas to rotate, thereby increasing the resistance of the main flow, altering the pressure of the combustion chamber, and adjusting the generation rate of combustion gas. Blatter and Keranen (1970) developed a vortex valve and achieved a flow modulation ratio of 3.46:1 when the pressure ratio of the control flow to the main flow was 1.7 in seven hot tests. Theoretical and scaled studies on vortex valve SRM conducted by Walsh et al. (1971) revealed that a small amount of control flow could contribute to a wide thrust modulation range; in these studies, the variation amplitude of pressure in combustion chamber reached 550%, which is 230% higher than the theoretical value. Greenberg and Wolff (1975) proposed a parameter calculation method for a vortex valve SRM, in

which cold flow is used to adjust thrust; the calculation results agreed well with the experimental results. Brodersen and Papadopoulos (1981) performed a theoretical analysis and experimental study on structure design of vortex valves and obtained a maximum modulation ratio of 9:1 by using helium and nitrogen as control flow and main flow, respectively. Natan *et al.* (1982) mainly investigated the influence of oxygen content in control flow and mass flow ratio of control flow to main flow on the modulation performance of vortex valve SRM with variable thrust. Zhang *et al.* (1996) conducted theoretical research on the design parameters of vortex valve SRM with variable thrust, established a computational model, and obtained meaningful conclusions. Guo *et al.* (1996) investigated how control flow, such as high-temperature combustion gas, nitrogen, and air, influences the modulation performance of vortex valve SRM with variable thrust and concluded that the modulation performance of high-temperature control flow is higher than that of low-temperature control flow. Lin *et al.* (2002) simulated the performances of two vortex valves by using CFL3D codes developed by NASA Langley Research Center; their results showed that the geometric shape of a vortex valve significantly influences on its modulation performance.

In related research on vortex valve SRM with variable thrust, relatively few studies explore the adjustment mechanism and flow process. Lewellen *et al.* (1969) studied the influence of swirl flow on the flow at the nozzle throat, and established a flow analysis model on the basis of the experimental results. The presicted results agreed well with experimental results for the maximum tangential Mach number in a vortex tube. The presicted results could also effectively indicate the increasing pressure in the combustion chamber during motor rotating. However, significant differences exist between the increasing amplitudes. It can predict the control flow rate when the pressure of the main flow drops significantly, but it can not forecast the control flow rate when the main flow is shut off. The incompressible, stable and axisymmetric flow in short vortex chamber of typical vortex valve was studied by Wormley (1969). The interaction between the main vortex core flow and the viscous chamber end wall boundary layers was established with the aid of flow visualization photographs. Bichara and Orner (1969) derived a model that can predict the steady-state input-output characteristics of vortex amplifiers operating in incompressible flow; they correlated this model with experimental data to affect prediction of the influence of operating fluid properties and critical dimensions of vortex valves on the valve characteristics. Woolhouse *et al.* (2001) evaluated the performance of a fluidic vortex amplifier by using computation fluid dynamics (CFD) simulation and model tests with ambient air. Although some discrepancies were found between the simulation and test data, the design and performance trends were successfully simulated. An important feature of CFD is the occurrence of a weak time-dependent flow structure, particularly with the Reynolds stress

model. Jawarneh *et al.* (2005) presented a study of flow in a jet-driven vortex chamber for a wide range of Reynolds numbers, contraction ratios, inlet angles, areas, and aspect ratios. The salient properties of flow and the influence of nondimensional parameters on the pressure coefficient and vortex core size were obtained. Norton *et al.* (1969) established a theoretical model for the rotating, inviscid, adiabatic, and compressible flow of perfect gas in converging passages and corrected the model with the effect of viscous dissipation. They also studied the effect of vortex-nozzle interaction and vortex choking on mass flow rate through a choked nozzle by using a rotating motor that employs air. Gany *et al.* (2005) theoretically studied the swirl flow in a choked nozzle. A novel analysis model for isentropic axisymmetric swirl flow based on one-dimensional compressible flow theory was established. The choking criterion was similar to that for one-dimensional nonswirling flows. Results showed that swirl intensity and type affect the distribution of Mach number at the throat and that mass flow rate decreases with increasing swirl intensity for fixed stagnation conditions. Holten *et al.* (2007) presented an analytical theory for a vortex flow through a Laval nozzle and found that the total velocity reaches sonic conditions upstream of the nozzle throat and that the axial velocity is equal to the local speed of sound in the nozzle throat. Martinelli *et al.* (2007) conducted an experimental analysis of the instability of the precessing vortex core in a free swirling jet of air at ambient pressure and temperature by using laser Doppler velocimetry and PIV. Results showed that turbulence intensity is not dependent on swirl parameter. Vatistas *et al.* (2005) and Jawarneh *et al.* (2007) performed a theoretical study of the flow characteristics of a deference vortex chamber. The characteristics of the pressure drop and the core size were obtained, and the influence of geometric parameters on the flow field was determined. Matsuno *et al.* (2015) conducted research on the temperature separation and the flow behaviour in a vortex chamber and determined the influence of geometric parameters on temperature separation. Akhmetov and Akhmetov (2016) studied the flow structure in a vortex chamber by using flow visualization and obtained the distributions of the azimuthal and axial components of velocity in the vortex chamber.

A number of studies have explored flow in a vortex chamber, the influence of swirl on the flow of the nozzle, and the thrust modulation performance of a vortex valve variable-thrust solid rocket motor. However, research on the modulation mechanism and flow process analysis of vortex valve is limited. The working principle of a vortex valve variable-thrust solid rocket motor has been introduced roughly in previous literatures. Nevertheless, the thrust modulation mechanism and the influence of swirl on the operation of the motor still need to be studied. Hence, in the current work, the swirl characteristics of a vortex valve variable-thrust solid rocket motor were investigated through cold flow experiments and numerical simulation.
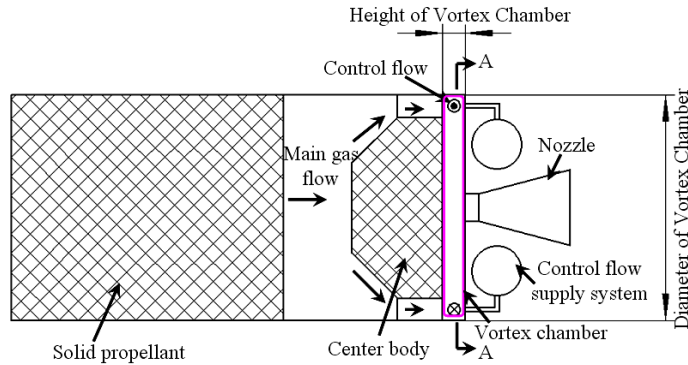
Fig. 1. Schematic diagram of vortex valve SRM with variable thrust.

2. VORTEX VALVE VARIABLE-THRUST SOLID ROCKET MOTOR

A vortex valve variable-thrust solid rocket motor is constructed by installing a vortex valve composed of a fluidic device and a control-flow injecting structure in front of the nozzle of an ordinary solid propellant rocket motor. A schematic of the motor is shown in Fig. 1 and Fig. 2. The main gas flow (or supply flow) generated by the main motor enters vortex chamber after it is adjusted to axial direction through the center body. It then mixes with the tangential control flow from the control flow supply system. As a result of the control flow with angular momentum, the flow swirls, pressure gradient appears, flow resistance increases, the pressure of the main motor combustion chamber rises, and the motor mass flow rate changes. Eventually, the motor thrust changes. In sum, the flow in a vortex chamber and the performance of the nozzle mainly determine the performance of thrust modulation. Hence, the flow characteristics in the vortex chamber, throat, and divergent section are the main factors that affect the performance of thrust modulation and the main approaches to reveal the mechanism of thrust modulation.
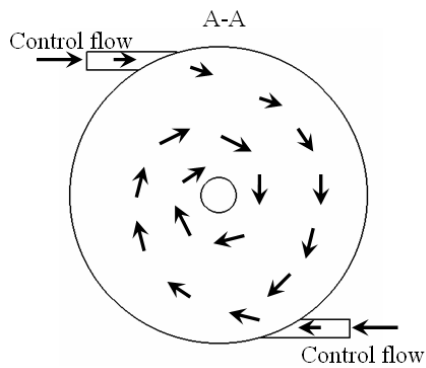
Fig. 2. Schematic diagram of flow in A-A cross section.

3. COLD FLOW TEST

3.1 Experiment System

A cold flow experimental system based on PIV was established to intuitively understand the flow in a vortex chamber and to calibrate the numerical model. The experimental system mainly consists of analog gas source of supply flow and control flow, a tracer particle broadcast system, a PIV test system, a measurement and control system, and some valves (Fig. 3). Nitrogen was selected as the analog gas source of supply flow to simulate the supply flow of combustion gas in the main motor. It was also selected as the analog gas source of control flow to simulate control flow. Al_2O_3 particles whose average diameter was 10 μm were sprayed by the tracer particle broadcast system and used to show the physical form of the flow field. The PIV test system made by TSI Corporation was used to collect and process the flow field information in the vortex chamber. The measurement and control system was used to control valve and collect pressure signals.

3.2 Experiment and Result Analysis

As the burning rate pressure exponent of propellant cannot be simulated by using nitrogen, the experiment could only simulate a process state and not a changing process. For the structure of flow field, the morphological characteristics are consistent regardless of the amount of pressure. To obtain a distinct flow field structure of the vortex chamber, we set the pressure of gas source to low. The test conditions are shown in Table 1.

Table 1 Cold flow Test conditions

	Pressure of supply flow /MPa	Pressure of control flow /MPa
Test 1	0.7	0.8
Test 2	0.7	0.75

The geometrical parameters involved in this experiment are as follows. The height and diameter of the vortex chamber were 10 and 100 mm, respectively. The diameter of the control flow injector was 3 mm. The diameter of the vortex chamber outlet was 10 mm. The vortex chamber comprised two injectors.

The velocity vector diagrams are shown in Figs. 4 and 5, which denote a stable vortex structure. The tangential velocity in the vortex chamber increased
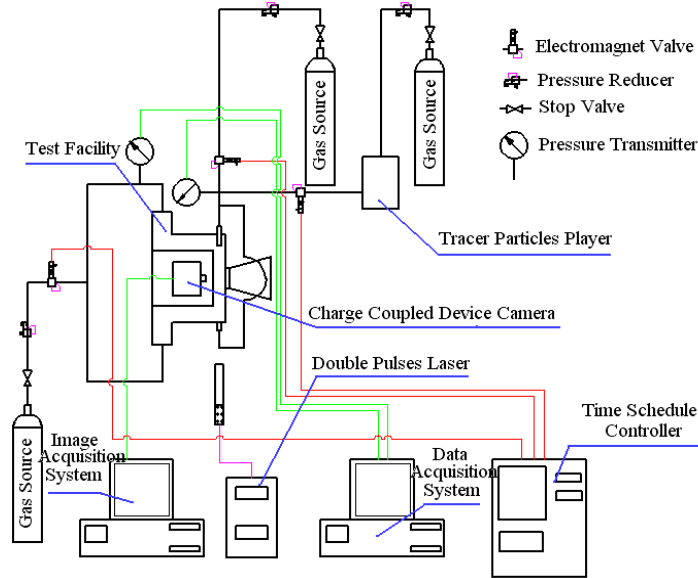
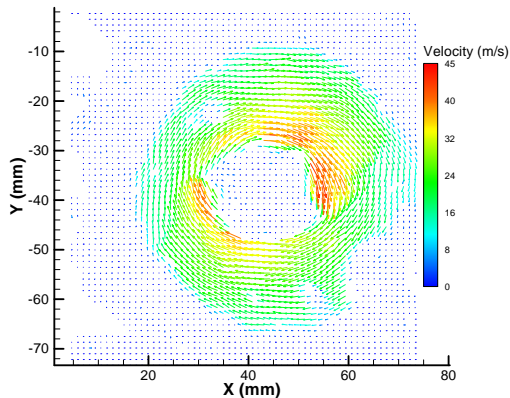**Fig. 3. Schematic diagram of cold flow experimental system.**

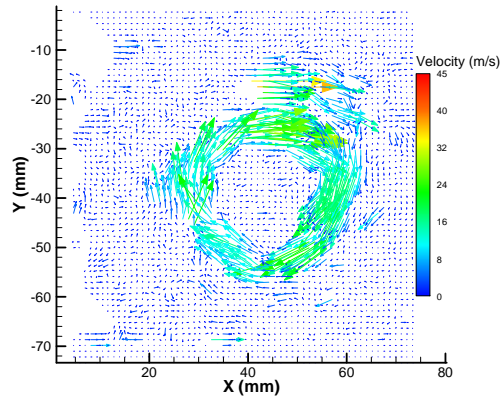**Fig. 4. Velocity vector diagram of test 1.**


Fig. 5. Velocity vector diagram of test 2.

with the decrease of the radius and began to decease near the outlet. A low-velocity zone appeared consequently. The strong swirl appears in only a certain part of the whole vortex chamber. The flow structure in the vortex chamber is similar to that in a complex Rankine vortex. Compared with the tangential velocities in test 2 in Fig. 5, the tangential velocities in test 1 in Fig. 4 were obviously higher. In other word, increasing the pressure of control flow improves the strength of swirl flow, that is, increasing the angular momentum in the vortex chamber can help improve swirl strength.

4. NUMERICAL COMPUTATION METHOD
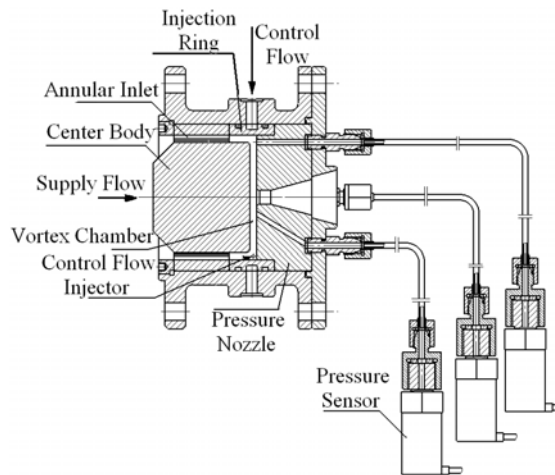
4.1 Computation Model

The FLUENT CFD simulation software of ANSYS Corporation was adopted in the numerical calculation. Some assumptions were made in the numerical calculations. The flow was adiabatic isentropic flow. The gas could be reasonably considered as ideal gas, and the mixed gas was an ideal gaseous mixture. Chemical reactions were not considered. The three-dimensional Reynolds-averaged Navier-Stokes equation and SST k-ω turbulence model were adopted, the convection term was discretized using an upwind scheme, the viscous term was discretized using central difference scheme, the time term was discretized using second order backward difference scheme, and the finite volume method was adopted to analyze the flow (Yu *et al*. (2007); Wei *et al*. (2017)). Structured and unstructured hybrid mesh methods were adopted, and the local meshes at the injector were refined. The boundary conditions were set as follows: the mass flow rate inlet was used for the supply flow, the pressure inlet was used for the injector of control flow, the pressure outlet was used for the nozzle exit, and a no-slip condition was used for the wall surface. When the control flow was injected into the vortex chamber, the combustion chamber pressure increased and led to the rise of the inlet mass flux. The mass flux in the
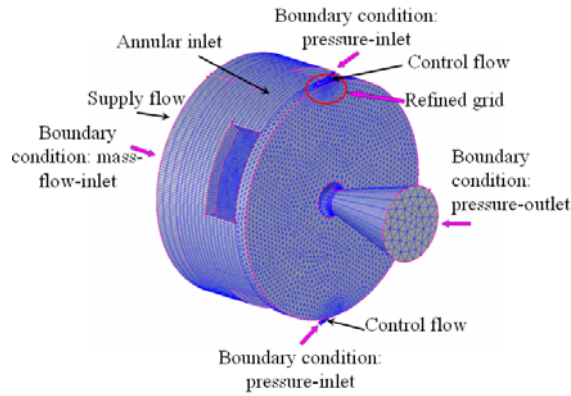
Fig. 6. Schematic diagram of calculation model.

**Fig. 7. Experiment device to measure pressure distribution.**

boundary conditions of supply flow was relevant to burning rate and was embedded in the computational model by using UDF (Fluent6.3 UDF Manual (2006)). "DEFINE_PROFILE" was added to the solver. At the end of every calculation step, the pressure of the supply flow was obtained, and the UDF "DEFINE_PROFILE" was called to calculate the mass flow rate. After the completion of all calculations, the solver continued to the next time step. The mass flow rate was calculated with formula $\dot{m} = \rho_p A_p a p_c^n$. The sketch map of the calculation structure and the boundary conditions are shown in Fig. 6.

4.2 Model Validation

To evaluate the applicability and accuracy of the model, we compared the simulated results of the pressure of the combustion chamber and the pressure distribution of the vortex chamber with the experimental results. The experiment system was described briefly in Wei *et al*. (2017). The experiment device for measuring the pressure distribution of the vortex chamber is shown in Fig. 7. The experimental results of pressure distribution are shown in Fig. 8. The end-burning propellant grain used in the tests was non-aluminized propellant. The burning rate of the

propellant was calculated according to the burning rate formula $r = 2.267 p_c^{0.6}$. The combustion temperature of the propellant was $T_f = 1789$ K. The diameter of the burning surface was 178 mm. The control flow used in the test was compressed nitrogen with a temperature, mass flow rate and pressure of 293 K, 0.104 kg/s and 8.84 MPa, respectively. The diameter and the height of vortex chamber were 90 and 3 mm, respectively. The diameter of the control flow injector was 2 mm, and two control flow injectors were equipped in the vortex chamber. The diameter of the nozzle throat was 10 mm. The pressures at distances of 12 and 18 mm from the central axis in vortex chamber were measured. Fig.8 shows good agreement between the change trends of numerical and experimental results. The numerical result was slightly higher than the experimental result with a maximum error of 9.5%. The heat loss was low in the numerical calculation because the heat loss during the mixing of the flows, the heat transfer to the shell and flow loss were neglected in modeling, and the wall of the experimental motor was thick without thermal insulation. A comparison of the experimental and numerical values of chamber pressure was presented in Reference Wei *et al*. (2017). The results of the numerical calculation

in the current work were slightly higher than those in the experimental data with a maximum error of 9.48%. Hence, the model can be effectively used to study the vortex valve variable-thrust solid rocket motor, and the numerical results are credible with acceptable precision.
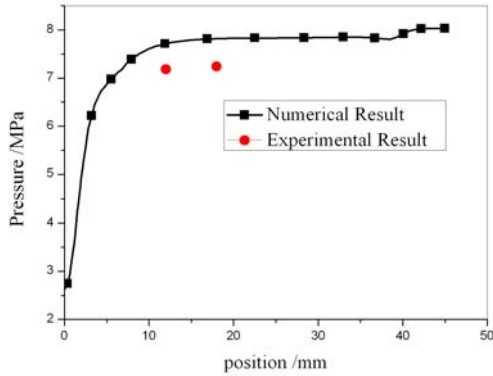

Fig. 8. Comparison of numerical and experimental results of pressure distributions.

5. FLOW CHARACTERISTICS ANALYSIS

The typical flow field streamlines of the vortex valve are shown in Fig. 9. The flow characteristics in the motor can be seen clearly. The situation before modulation is shown in Fig. 9 (a); here, the supply flow flows into the vortex chamber through the center body, proceeds radially toward the outlet in the vortex chamber, and finally flows out through the nozzle. No swirling flow occurs in the vortex chamber. The situation after modulation is shown in Fig. 9 (b); here, the tangential control flow is mixed with the supply flow and then rotated. Swirl flow occurs in the vortex chamber due to the viscous effect and conservation of angular momentum, and it strengthens gradually toward the center of the vortex chamber. The swirl flow maintains its stable vortical structure from the vortex chamber to the throat. The swirl strength seriously weakens as it enters the divergent section, and the effect of the swirl flow decreases rapidly. In other words, swirl flows are generated in the region between the vortex chamber and the nozzle throat, and they weaken quickly in the divergent section. In sum, an obvious change occurs in the motor after modulation, that is, swirl flow occurs, and the velocity has a large tangential component. To study the flow characteristics and reveal the mechanism of thrust modulation in the vortex valve variable-thrust solid rocket motor, we analyzed the flow characteristics in vortex chamber, throat, and divergent section of the nozzle. The main structural parameters of the vortex valve are as follows: the diameter and the height of vortex chamber were 90 and 5 mm, respectively, the diameter of the control flow injector was 2 mm, two control flow injectors

were equipped in the vortex chamber, and the diameter of the throat is 10 mm. The gas generated by the pressure distribution of the experimental motor was used as supply flow. Compressed nitrogen was used as the control flow. The total temperature and total pressure were 293 K and 11.24 MPa, respectively.


(a)

(b)
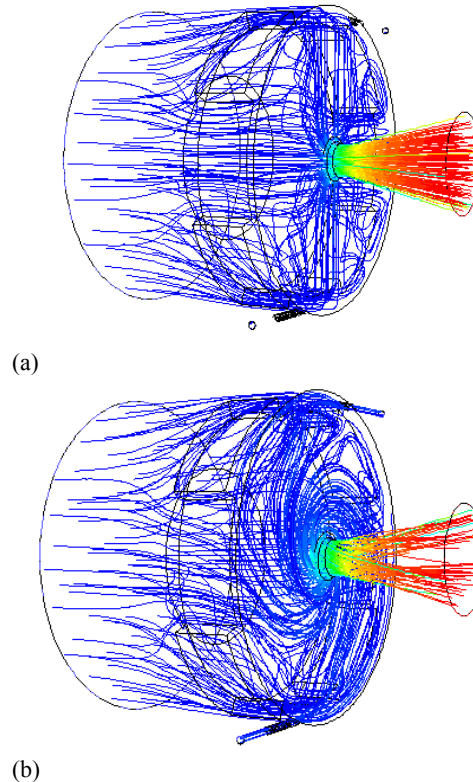
Fig. 9. Streamlines of flow field, before injecting control flow ((a) and after injecting control flow (b)).

5.1 Flow Characteristics in Vortex Chamber

The vortex chamber is the main region where the supply flow and control flow are mixed and momentum is exchanged. The velocity vector diagrams in the middle section of the vortex chamber before and after the injection of the control flow are shown in Fig. 10. As shown in Fig. 10 (a), the flows move mainly along the radial direction in the vortex chamber in the absence of control flow and then flow into the nozzle along the axial direction at the exit of vortex chamber. As shown in Fig. 10 (b), after the addition of control flow, momentum exchange becomes the main action for the supply flow and control flow at the outer layer of the vortex chamber, and the swirl flow dominates at the center. When the swirl flow is close to the center, the swirl strength is high. A low-velocity zone then appears in the center. This result conforms to the velocity distribution of the complex Rankine vortex. The simulated results agree well with those of the cold flow experiment and confirm the reliability of the numerical simulation.
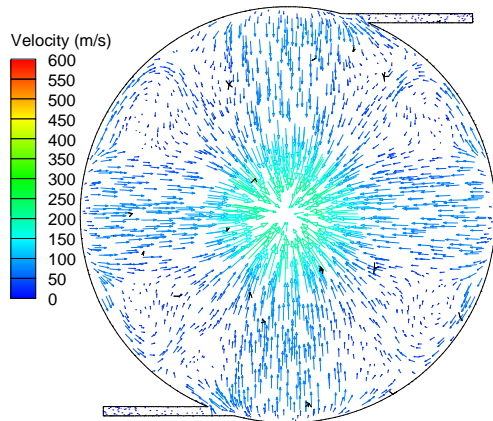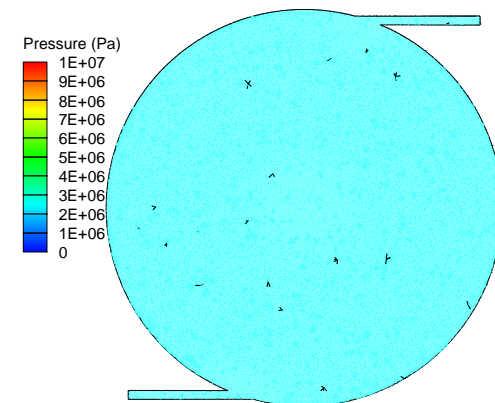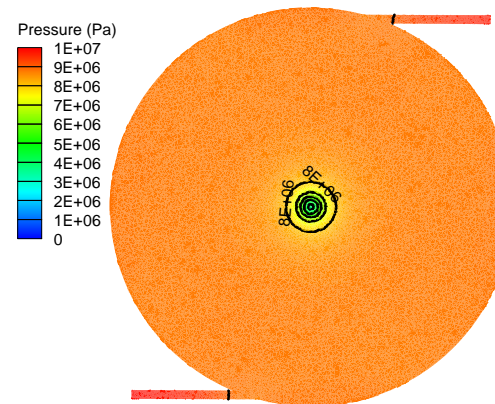
(a)
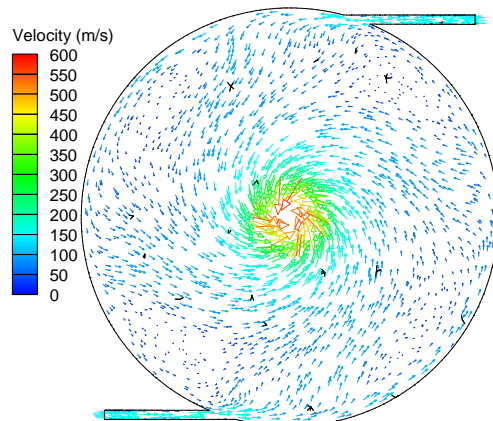
(b)

Fig. 10. Velocity vector diagram in the middle section of vortex chamber, ((a) before injecting control flow, (b) after injecting control flow).

Figures 11 and 12 show the distributions of pressure and density in the middle section of vortex chamber before and after the injection of control flow. The flow in the vortex chamber is uniform before the injection of control flow, as shown in Fig. 11 (a). The pressure in the vortex chamber decreases gradually from the outer layer to the center, i.e., pressure gradient exists and drastically changes as in approaches the center, as shown in Fig. 11 (b). The density distribution in the vortex chamber after the injection of control flow can be divided into three zones. The density at the outer layer is uneven, and this zone is relatively small. The density at the middle zone is uniform, and this zone is relatively large. The density at the center is extremely small, and this zone is the smallest, as shown in Fig. 12 (b). Fig. 13 shows the radial distribution of density in the middle section of the vortex chamber. The density is changed greatly only at the small zone of the center and at the zone where the two flows begin to mix. The change amplitude in most areas of the vortex chamber is minimal at approximately 7.14%. According to the flow characteristics in the vortex chamber, the mixing of the two flows and the momentum exchange mainly take place at the outer layer. The flow translates into an incompressible flow as the mixing process ends, and then a rarefied gas area

appears in the small central zone of the vortex chamber. The rarefied gas area hinders gas from flowing to the exit of the nozzle and reduces the exit area of the vortex valve, i.e., the effective flow area of the throat. According to the principle of SRM, under other given conditions, the pressure in the combustion chamber increases while the throat area decreases. Increasing the pressure in the combustion chamber can improve the mass flow rate generated by the combustion of the propellant and thereby improve its thrust. Thrust modulation can be achieved. In sum, the size of vortex core serves as a main influence factor for thrust modulation. However, the size of the vortex core needs to be determined.

(a)

(b)

Fig. 11. Distributions of pressure in the middle section of vortex chamber ((a) before injecting control flow, (b) after injecting control flow).

The complex Rankine vortex consists of a quasi-forced vortex in the vortex core and a quasi-free vortex outside of the vortex core. In the vortex core, flow viscosity dominates, and tangential velocity increases linearly to the maximum value from the center to the outside and then gradually decreases while the radius increases. Generally, the radius of vortex core corresponds to the maximal tangential velocity. However, it cannot be calculated theoretically, and it can only be obtained by measuring the inflection point of the velocity curve. The distribution of the resultant velocity, axial

velocity, tangential velocity, and radial velocity of gas in the middle section of the vortex chamber are shown in Fig. 14.
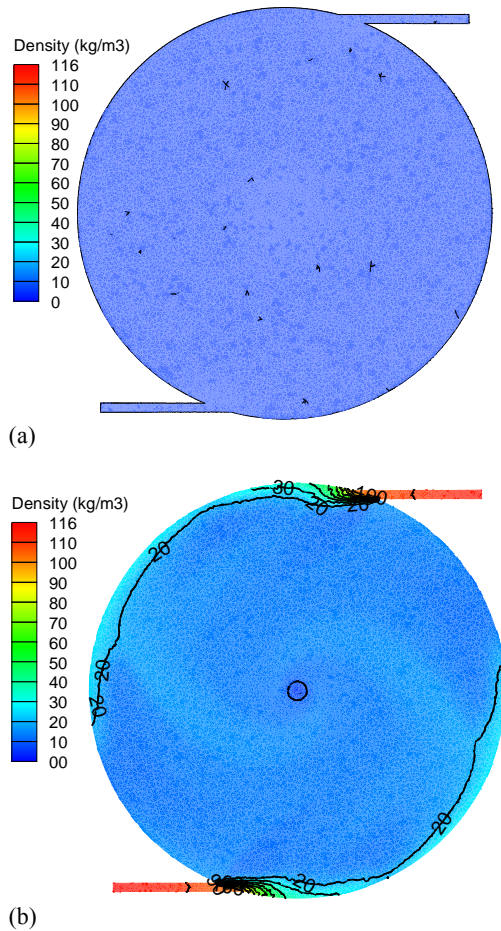

(a)

(b)

Fig. 12. Distributions of density in the middle section of vortex chamber ((a) before injecting control flow, (b) after injecting control flow).
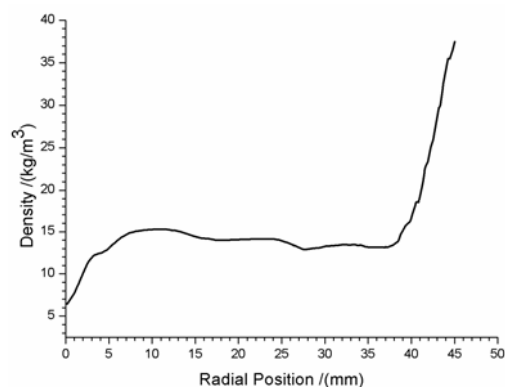

Fig. 13. Radial distribution of gas density in vortex chamber.

Figure 14 shows that the distribution of the tangential velocity in the vortex chamber is consistent with that of the complex Rankine vortex. Axial velocities are almost zero, except in some zones. The axial velocity is not zero in the circular channel with a radius of 10 mm and the region corresponding to the annular inlet. In the

circular channel, the axial velocity increases while radius decreases. Furthermore, the flow in the vortex chamber shows three different characteristics, and the vortex chamber can be divided into three regions. This feature is similar to that of the vortex chamber model built by Bichara and Orner (1969). Radial velocity increases while radius decreases and then decreases rapidly in some zones whose diameter is equal to that of the nozzle throat. The radius of the vortex core is 2.2 mm under this condition, as shown in Fig. 14. In combination with a previous density analysis, this work shows that the gas density in the vortex core region is extremely low, resulting in the reduction of the flow capacity of the throat. That is to say, the generation of the vortex core reduces the effective area of the throat. The resultant velocity changes obviously within the zone whose radius is nearly equal to the exit diameter. The changing trend of the resultant velocity is almost consistent with that of tangential velocity, and it indicates the dominant role of tangential velocity in the vortex chamber.
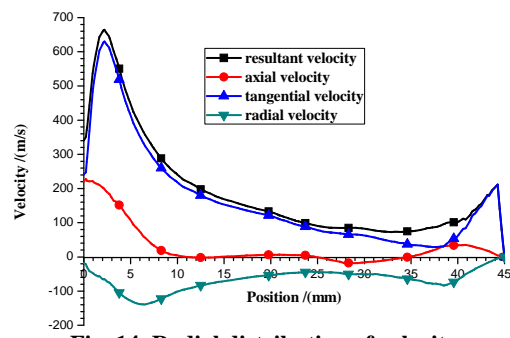

Fig. 14. Radial distribution of velocity component in the middle section of vortex chamber.

5.2 Flow Characteristic at the Throat

The research results of Holten *et al.* (2007) showed that axial velocity at the throat is equal to the local speed of sound when swirl flow runs into a choked Laval nozzle and that the resultant velocity reaches supersonic speed at the upstream of the nozzle. In the present study, the convergent section of the nozzle with a 180º convergence angle was designed to achieve the required high adjustment performance of the vortex valve variable-thrust solid rocket motor. The entrance of the throat was rounded with R2mm, and the flat section length of the throat was 3mm. Understanding how swirl flow affects the flow at the throat can support the effort to reveal the mechanism of thrust modulation. The longitudinal section of the vortex valve is shown in Fig. 15.

Figure 16 shows the Mach number at the throat and its change trends along a straight line which is parallel to and 3mm away from the X-coordinate axis. The line is in the stable region and extends beyond the vortex core region. Ma stands for the Mach number and is defined as the

ratio of local velocity to local speed of sound. Ma_x stands for the axial Mach number and is defined as the ratio of axial velocity to local speed of sound. "modulated Ma" and "modulated Ma_x" stand for the Mach number and the axial Mach number, respectively, after the control flow is injected into the vortex chamber. " unmodulated Ma" stands for the axial Mach number before the control flow is injected into the vortex chamber. Before and after modulation, axial Mach number 1 always appears in the range of 64.2-64.4 mm along the X-coordinate axis, and the interval belongs to the flat section of the throat. After modulation, the Mach number of resultant velocity reaches 1 when X value is less than 62.8 mm. The results are consistent with those in Holten *et al*. (2007). Hence, for the vortex valve variable-thrust solid rocket motor, whether the throat is choked can be determined according to whether the axial velocity equals local sound velocity.
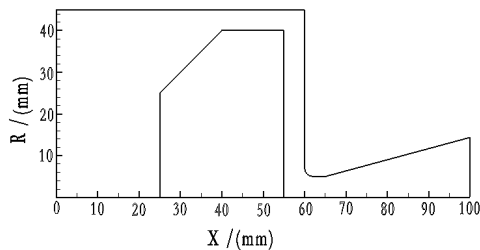

Fig. 15. Schematic diagram of longitudinal section of vortex valve.
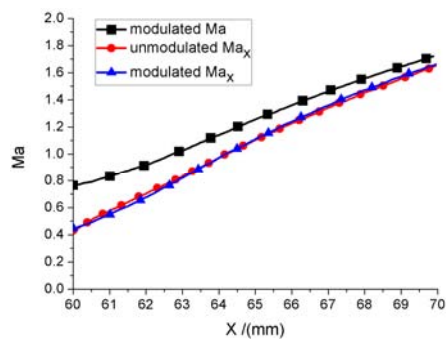

Fig. 16. Distribution of Mach number along a straight line which is parallel to and 3mm from X-coordinate axis.

5.3 Flow Characteristic in Divergent Section of Nozzle

The divergent section of the nozzle is the region where flow is accelerated continuously and heat energy is transformed into kinetic energy. How the swirl flow in the divergent section affects the thrust performance of motor. Fig. 17 shows the distributions of tangential velocity along the radial direction at different axial positions in the vortex chamber, throat, and divergent section of the nozzle after the injection of control flow. Fig. 18 shows the distribution of tangential velocity in the middle section of the vortex chamber after the injection of

control flow. Fig. 17 and 18 show that tangential velocity decreases along the axial direction and is extremely fast in the vortex chamber and the nozzle throat with minimal change. However, it decreases obviously and changes sharply in the divergent section. In the vortex and throat, the vortex core can be distinguished clearly, its radius hardly changes, and its boundary is no longer clear in the divergent section.
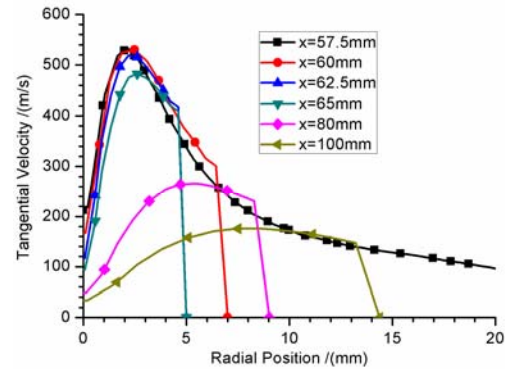

Fig. 17. Distributions of tangential velocity along radial direction at different axial positions.
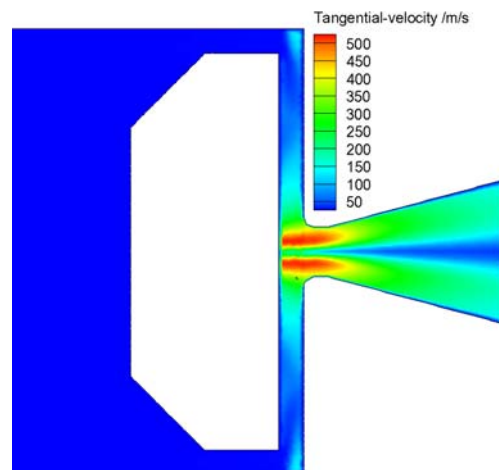

Fig. 18. Distribution of tangential velocity of the motor.

Figure 19 shows the distribution of the static pressure in the vortex valve. Obvious pressure changes are present in the central region of the vortex chamber. A low-pressure zone appears around the axis, and it continuously extends to the center of the divergent section. The pressure near the axis is lower than the pressure in other locations at the one cross section. The generation of the low pressure zone is due to the present of the vortex core. Hence, the effect of the inlet structure of supply flow on its flow can be neglected in modeling the vortex valve variable-thrust solid rocket motor. As a result of the low pressure zone near the central axis, the thrust generated by pressure decreases leads to thrust loss. Consequently, performance declines.
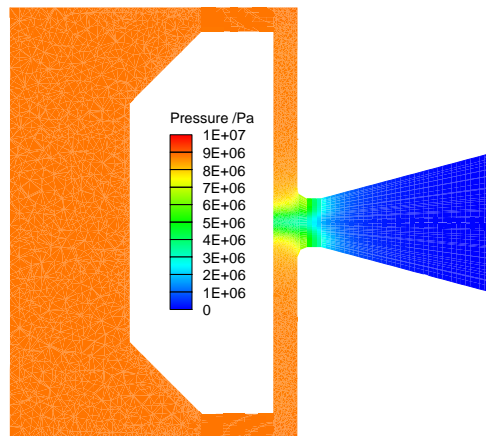
Fig. 19. Distribution of pressure for flow field in vortex chamber.

6. CONCLUSION

Through a cold flow experiment and numerical simulation of the flow field in the vortex valve variable-thrust solid rocket motor, the flow characteristics in the vortex chamber, nozzle throat and divergent section were obtained. The mechanism of thrust modulation can be explained as follows. The flow flux at the nozzle throat decreases, and the effective area of the throat is reduced because of a low-density zone, i.e., the vortex core generated by swirl flow. The performance degradation due to swirl flow can be mainly attributed to the low-pressure zone near the central axis of the divergent section, which lowers the thrust generated by differential pressure and limits the working capacity of gas flow. The flow in the vortex chamber conforms to the swirl flow of the complex Rankine vortex and includes three evident flow regions: mixture of supply flow and control flow, quasi-free vortex and quasi-forced vortex. The work provides a theoretical foundation for the modeling of the vortex valve variable-thrust solid rocket motor.

REFERENCES

Akhmetov, D. G. and T. D. Akhmetov (2016). Flow structure in a vortex chamber. *Journal of Applied Mechanics and Technical Physics* 57(5), 879-887.

Alon, G., M. Mor and C. Goldman (2005). Analysis and characteristics of choked swirling nozzle flows. *AIAA Journal* 43(10), 2177-2181.

Bichara, R. T. and P. A. Orner (1969). Analysis and modeling of the vortex amplifier. *Transactions of ASME, Series D, Journal of Basic Engineering* 91(4), 755-763.

Blatter, A. and T. W. Keranen (1970). A vortex valve for flow modulation of 5500°F gas. *Journal of Spacecraft and Rockets* 7(2), 169-174.

Brodersen, R. K. and J. G. Papadopoulos (1981). Hot gas control system design and vortex valve tests. *IEEE Transactions on Automatic Control* 26(3), 625-637.

David, J. N., B. W. Farquhar and J. D. Hoffman (1969). An analytical and experimental investigation of swirling flow in nozzles. *AIAA Journal* 7(10), 1992-2000.

Fluent 6.3 UDF Manual (2006). Fluent Inc.

Fulvio, M., A. Olivani and A. Coghe (2007). Experimental analysis of the precessing vortex core in a free swirling jet. *Experiments in Fluids* 42(6), 827-839.

Georgios, H. Vatistas, A. M. Jawarneh and H. Hong (2005). Flow characteristics in a vortex chamber. *The Canadian Journal of Chemical Engineering* 83, 425-436.

Greenberg, I. and H. Wolff (1975). Cold flow evaluation of parameters influencing thrust modulation by a fluidic vortex valve. *Israel Journal of technology* 13, 73-81.

Holten, T., A. Jaeken, M. M. J. Schoones and M. M. Heiligers (2007). Throttling a laval nozzle by a vortex: an analytical theory *AIAA* 1282.

Jawarneh, A. M., P. Sakaris and H. G. Vatistas (2007). Experimental and analytical study of the pressure drop across a double-outlet vortex chamber. *Transactions of the ASME, Journal of Fluids Engineering* 129, 100-105.

Jawarneh, A., G. H. Vatistas and H. Hong (2005). On flow development in jet-driven vortex chambers. *Journal of Propulsion and Power* 21(3), 564-570.

Lewellen, W. S., W. J. Burns and H. J. Strickland (1969). Transonic Swirling Flow. *AIAA Journal* 7(7), 1290-1297.

Matsuno, Y., Y. Fukushima, S. Matsuo, T.Hashimoto, T. Setoguchi and H. Dong Kim (2015). Investigation on temperature separation and flow behaviour in vortex chamber. *Journal of Thermal Science* 24(2), 149-154.

Natan, B., A. Gany and H. Wolff (1982). Thrust modulation of solid propellant rockets by a fluidic vortex valve with secondary combustion. *Acta Astronautica* 9(12), 703-711.

Ray Sing, L., N. Hariharan and T. Brogan (2002, June). Analysis of fluidic vortex valves for airflow control in combustors *AIAA* 2946.

Walsh, R. F., W. S. Lewellen and D. B. Stickler

(1971). A solid-propellant rocket motor modulated by a fluidic vortex valve. *Journal of Spacecraft and Rockets* 8(1), 77-79.

Woolhouse, R. J., J. R. Tippetts and S. B. M. Beck (2001). A comparison of the experimental and computational modeling of the fluidic turn-up vortex amplifier at full and zero swirl conditions. *Journal of Mechanical Engineer Science* 215(8), 893-903.

Wormley, D. N. (1969). An analytical model for the incompressible flow in short vortex chambers. *Transactions of ASME, Series D, Journal of Basic Engineering* 91(2), 264-272.

Xianggeng, W., L. I. Jiang and H. E. Guoqiang (2017). Influence of structural parameters on the performance of vortex valve variable-thrust solid rocket motor. *International Journal of Turbo and Jet-Engines* 34(1), 1-9.

Xiaojing, Y., H. Guoqiang, L. Jiang, L. Yang and W. Xianggeng (2007). Numerical analysis of flow in variable thrust SRM based on vortex valve *AIAA* 5801.

Zhang, W., J. Guo, L. Y. Xie, G. F. Zhang and S. Q. Jiao (1996). Thrust random modulation numerical simulation for SRM *AIAA* 2596.